NASSP ACB - Data Analysis (AR Sco)

May 2025

K. Elliott - ELLKIR005

Aim

The aim of this project is to analyze a photometric light curve of the magnetic cataclysmic variable (mCV), AR Scorpii (AR Sco).

Introduction

A cataclysmic variable (CV) is defined as a compact white dwarf (WD) star that is accreting material from the larger companion star that has overfilled its Roche Lobe in the binary system. A third of the accreting WD systems found have been observed to host a magnetic WD, thus creating a magnetic CV. Magnetic CV's can be further categorised into intermediate polars which have a magnetic field strength of $\approx 1 - 10$ MG, or polars which have a magnetic field strength of $\approx 10 - 240$ MG. Polars usually show the WD becoming tidally locked with the companion, while intermediate polars tend to show the WD spinning much faster than its orbital period [Rodriguez et al., 2025].

If the magnetosphere reaches out past the co-rotation radius, the magnetic field lines could sweep out and expel the diamagnetic blobs as they try to accrete. This acts as a 'propeller' expelling material and therefore energy from the system. This loss of energy causes the WD spin to slow down.

AR Scorpii (AR Sco) has been described as a non-accreting binary that hosts a rapidly spinning magnetic WD and a low-mass red dwarf star orbiting with a period of 3.56 hrs. It is believed to have a spin period of 1.97 min that is slowing down at a rate of $\frac{\dot{P}}{P} = 5.6 \times 10^6$ yr. If the WD slows down enough, it may become a polar system with a spin period equal to that of its orbital period [Rodriguez et al., 2025]. The spin frequency (ω) of the WD obviously does not equal the orbital frequency (Ω); this causes a beat frequency ($\omega - \Omega$) between the spin and orbital frequencies.

AR Sco has been referred to as a WD pulsar [Potter and Buckley, 2018] due to its bright, polarised pulsed flashes of synchrotron emission from an area near the magnetic poles; thought to have been powered by the spin-down of the WD [Gaibor et al., 2020, Stiller et al., 2018, Marsh et al., 2016, Pelisoli et al., 2022]. Potter and Buckley [2018] has suggested this synchrotron emission could be the result of electrons being injected into the WD magnetosphere and accelerating towards the poles. Through their simple geometric model Potter and Buckley [2018] found a 117 sec spin period, 118 sec beat period and a 3.6 hr orbital period.

Precession of the white dwarf spin axis may also be affecting the evolution of the beat pulse pairs [Garnavich et al., 2023]. The pairs have been seen to have changed from the primary peak being double the amplitude of the secondary peak to having nearly equal amplitudes over the span of a decade.

9/10

Method

The data was collected the 25th and 26th of May 2016 using the HIgh- speed-Photo-Polarimeter (HIPPO) [Potter et al., 2010] on the SAAO 1.9 m telescope as part of the paper by Potter and Buckley [2018].

The lightcurves in Fig. 1a and 1b shows the periodic nature of the target. The orbital period is most visible in the lightcurve, with almost a full period seen in the 4.7 hr observation on the 25th of May and almost 2 full periods seen in the 7.37 hr observation on the 26th of May [Potter and Buckley, 2018].

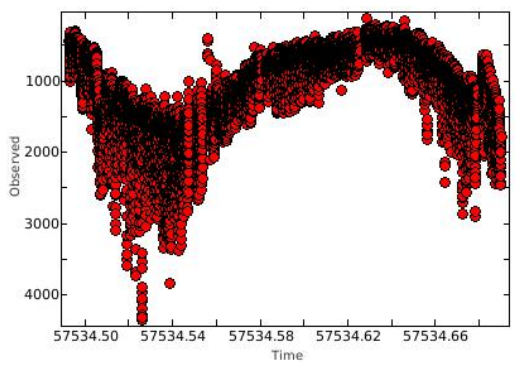

(a) Lightcurve showing observations on the 25th of May 2016

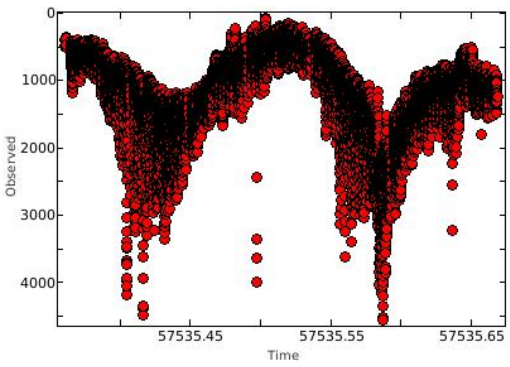

(b) Lightcurve showing observations on the 26th of May 2016

Using a program such as `Period04`, a Fourier transform can be applied to the lightcurve data to produce a periodogram. The Fourier transform allows us to convert our time domain lightcurves into the frequency domain in order to identify the main contributions to the observed waveform. The main contributor in the periodogram (highest peaked frequency, usually the orbital frequency) can then be subtracted from the original periodogram, and a new Fourier transform can be performed to produce an updated periodogram. This new periodogram can now show the finer details of the smaller contributors, such as the spin and beat frequencies. This process of subtracting the main contributor is repeated multiple times in order to find the most relevant frequencies.

`Period04` allows for parameter uncertainty estimation using Monte Carlo Simulations. This involves creating 100 simulated datasets with identical time data and magnitudes predicted by the last fit plus a Gaussian noise. The frequency and phase uncertainties have been uncoupled by shifting the time string until the 'average time' is zero. A linear least-squares calculation is then performed on each new dataset. Based on the distribution of 100 values for each of the parameters found, an uncertainty is found for each parameter.

Harmonics are defined as integer multiples of a fundamental frequency which arise when the Fourier transform tries to recreate the waveform. Therefore, we would expect to see the orbital frequency (Ω), spin frequency (ω), beat frequency ($\omega - \Omega$) and their harmonics in the periodogram produced.

9/10 There is a phenomenon known as aliasing which arises due to the data being sampled a day apart, which is below the Nyquist rate. This causes the smaller peaks seen across the periodogram.

Results

`Period04` is used to perform the Fourier transform where the average zero-point of 1163 cycles per day was subtracted to minimize the effect of any brightness difference between the two observations. The data is transformed using a sampling rate of 11079 cycles per day to include the majority of the frequency spectrum and plotted in Fig. 2. The most influential frequency contributors can be seen as tall spikes in the periodogram.

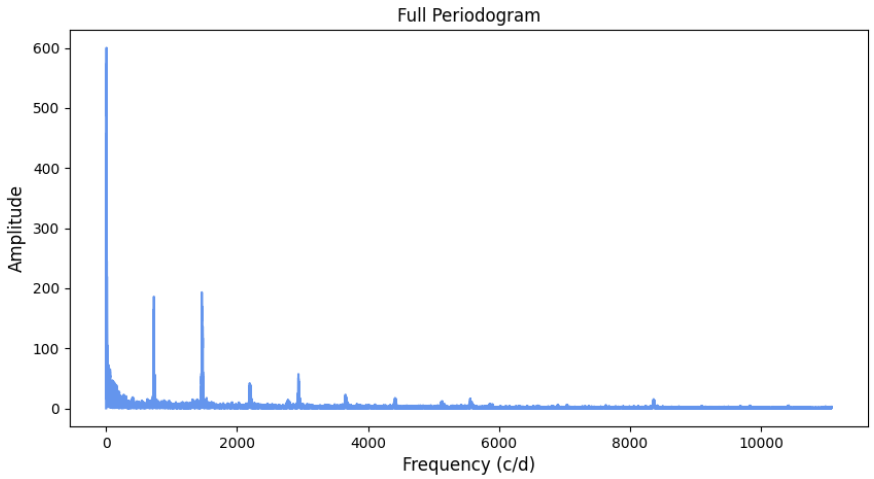

Figure 2: Periodogram showing the full frequency spectrum from 0 - 11079 cyces per day

`Period04` is used to fit frequency values to the maximum value of the largest Gaussian shaped hump. After each iteration, the contribution from this frequency is removed and the fit is repeated. This was performed on the data 30 times resulting in 30 frequencies which can be found in Tab. 2. These identified frequencies are compared with known literature and validated to remove any frequencies found in error.

A Least-Squares Regression can be calculated on the 30 frequencies in `Period04`, these uncertainties can be found in Table 1.

Table 1: Table showing the 16 identified frequencies and their associated errors

Index	Identity	Frequency (c/d)	Error (c/d)	Period (sec)
1	Ω	6.721	0.012	12855
2	2Ω	12.42	0.061	6956.5
3	3Ω	20.49	0.668	4216.7
4	$\omega - 2\Omega$	725.2	1.395	114.86
5	$\omega - \Omega$	731.0	0.013	118.19
6	ω	737.7	0.014	117.12
7	$2\omega - 3\Omega$	1456	7.115	59.341
8	$2(\omega - \Omega)$	1462	0.007	59.097
9	$2\omega - \Omega$	1469	0.004	58.816
10	2ω	1475	0.004	58.576
11	$3(\omega - \Omega)$	2193	0.013	39.398
12	$3\omega - 2\Omega$	2200	0.022	39.273
13	$3\omega - \Omega$	2206	3.527	39.166
14	$4\omega - 2\Omega$	2937	0.016	29.418
15	$4\omega - \Omega$	2944	6.269	29.348
16	4ω	2951	0.020	29.278

Looking at closer intervals such as in the figures below, the orbital, spin and beat frequencies can be distinguished as well as their harmonics. The one day aliasing can be seen clearly in these plots as the smaller sine-like wave along the larger amplitude humps.

The orbital frequency (Ω) and its harmonics ($2\Omega, 3\Omega$) can be distinguished in Fig. 3 at the frequencies found in Table. 1.

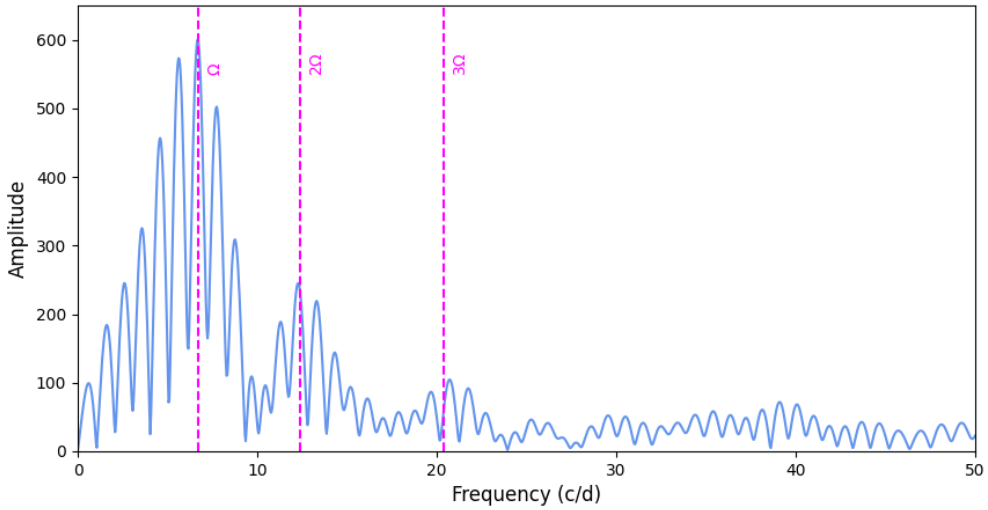

Figure 3: Periodogram showing frequencies between 0-50 cycles per day

The spin frequency (ω), beat frequency ($\omega-\Omega$) and it's harmonic ($\omega-2\Omega$) can be seen in Fig. 4 at the frequencies found in Table. 1.

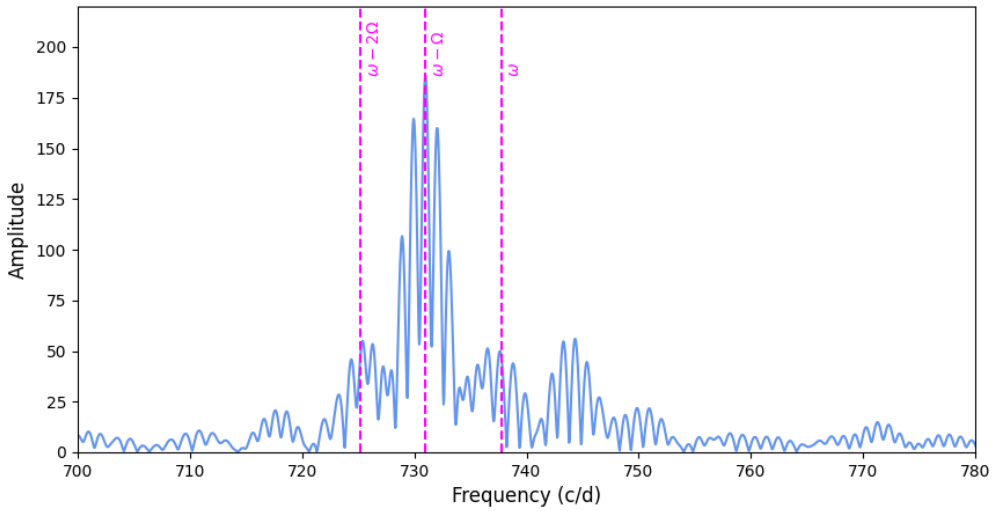

Figure 4: Periodogram showing frequencies between 700-780 cycles per day

Figures 5, 6 and 7 show the harmonics of the spin and beat frequencies which can be found in Table 1.

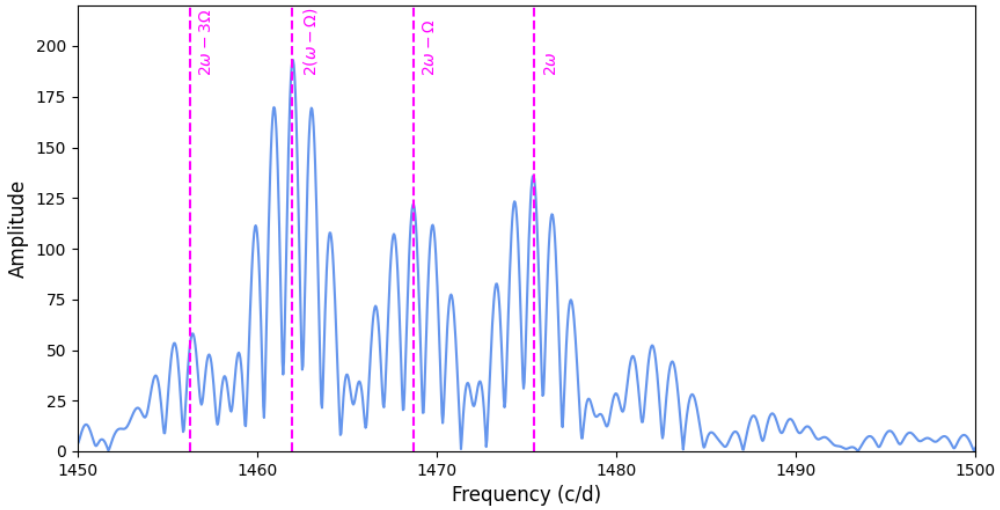

Figure 5: Periodogram showing frequencies between 1450-1500 cycles per day

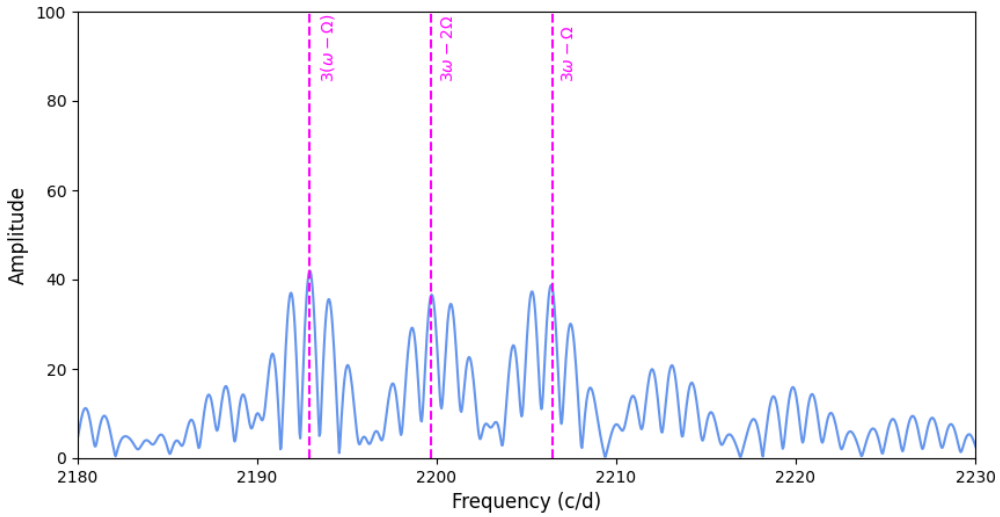

Figure 6: Periodogram showing frequencies between 2180-2230 cycles per day

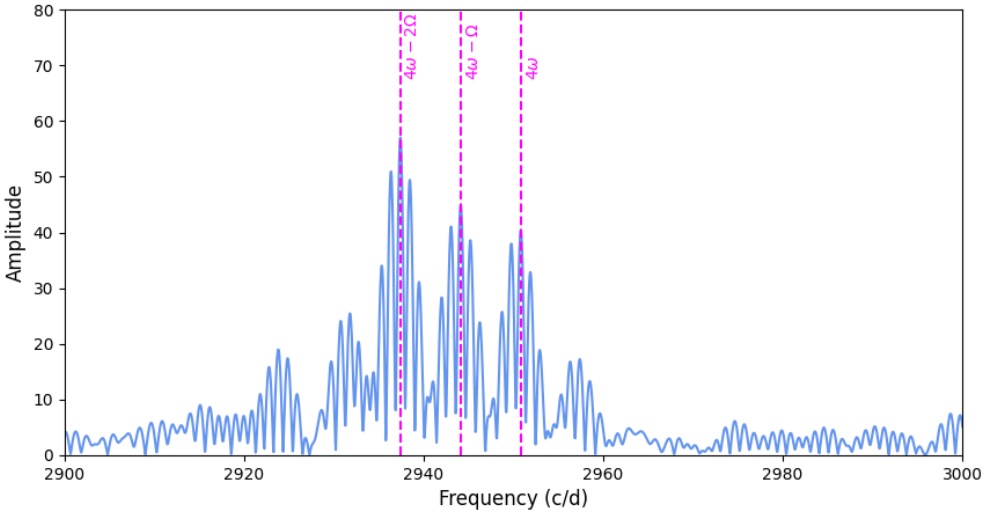

Figure 7: Periodogram showing frequencies between 2900-3000 cycles per day

9/10

Discussion

Interestingly 3ω was not identified. The orbital, spin and beat periods of 3.6 hr, 117.12 sec and 118.19 sec respectively agree very well with previous literature. They also show a low error in the identified frequency, 0.012, 0.014, 0.013 cycles per day respectively. At the time of these observations, the beat frequency is much larger than the spin frequency. Previous studies by Garnavich et al. [2023] suggest the beat frequency is double the amplitude of the spin frequency. This seems to be exaggerated in this study.

References

Y. Gaibor, P. Garnavich, C. Littlefield, S. Potter, and D. Buckley. An improved spin-down rate for the proposed white dwarf pulsar ar scorpii. *Monthly Notices of the Royal Astronomical Society*, 496(4):4849–4856, 8 2020. ISSN 0035-8711. doi: 10.1093/mnras/staa1901. URL https://doi.org/10.1093/mnras/staa1901.

P. Garnavich, S. Potter, D. Buckley, A. van Dyk, D. Egbo, C. Littlefield, and A. Greiveldinger. Rapid evolution of the white dwarf pulsar ar scorpii. *The Astrophysical Journal Letters*, 958(2):L22, 12 2023. ISSN 2041-8205. doi: 10.3847/2041-8213/ad0be7. URL https://doi.org/10.3847/2041-8213/ad0be7.

T. Marsh, B. Gänsicke, S. Hümmerich, F. Hambsch, K. Bernhard, C. Lloyd, E. Breedt, E. Stanway, D. Steeghs, S. Parsons, O. Toloza, M. Schreiber, P. Jonker, J. van Roestel, T. Kupfer, A. Pala, V. Dhillon, L. Hardy, S. Littlefair, A. Aungwerojwit, S. Arjyotha, D. Koester, J. Bochinski, C. Haswell, P. Frank, and P. Wheatley. A radio-pulsing white dwarf binary star. *Nature*, 537(7620):374–377, 9 2016. ISSN 0028-0836. doi: 10.1038/nature18620. URL https://doi.org/10.1038/nature18620.

I. Pelisoli, T. Marsh, S. Parsons, A. Aungwerojwit, R. Ashley, E. Breedt, A. Brown, V. Dhillon, M. Dyer, M. Green, P. Kerry, S. Littlefair, D. Sahman, T. Shahbaz, J. J Wild, A. Chakpor, and R. Lakhom. Long-term photometric monitoring and spectroscopy of the white dwarf pulsar ar scorpii. *Monthly Notices of the Royal Astronomical Society*, 516(4):5052–5066, 9 2022. ISSN 0035-8711. doi: 10.1093/mnras/stac2391. URL https://doi.org/10.1093/mnras/stac2391.

S. Potter and D. Buckley. Time series photopolarimetry and modelling of the white dwarf pulsar in ar scorpii. *Monthly Notices of the Royal Astronomical Society*, 481(2):2384–2392, 12 2018. ISSN 0035-8711. doi: 10.1093/mnras/sty2407. URL https://doi.org/10.1093/mnras/sty2407.

S. Potter, D. Buckley, D. O'Donoghue, E. Romero-Colmenero, J. O'Connor, P. Fourie, G. Evans, C. Sass, L. Crause, M. Still, O. Butters, A. Norton, and K. Mukai. Polarized qpos from theintegralpolar igrj14536-5522 (=swift j1453.4-5524). *Monthly Notices of the Royal Astronomical Society*, 402(2):1161–1170, 02 2010. ISSN 0035-8711. doi: 10.1111/j.1365-2966.2009.15944.x. URL https://doi.org/10.1111/j.1365-2966.2009.15944.x.

A. Rodriguez, K. El-Badry, P. Hakala, P. Rodríguez-Gil, T. Bao, I. Galiullin, J. Kurlander, C. Law, I. Pelisoli, M. Schreiber, K. Burdge, I. Caiazzo, J. van Roestel, P. Szkody, A. Drake, D. Buckley, S. Potter, B. Gaensicke, K. Mori, E. Bellm, S. Kulkarni, T. Prince, M. Graham, M. Kasliwal, S. Rose, Y. Sharma, T. Ahumada, S. Anand, A. Viitanen, A. Wold, T. Chen, R. Riddle, and R. Smith. A link between white dwarf pulsars and polars: Multiwavelength observations of the 9.36-minute period variable gaia22ayj. *Publications of the Astronomical Society of the Pacific*, 137(2):024202, 2 2025. ISSN 0004-6280. doi: 10.1088/1538-3873/adb0f1. URL https://doi.org/10.1088/1538-3873/adb0f1.

R. Stiller, C. Littlefield, P. Garnavich, C. Wood, F. Hambsch, and G. Myers. High-time-resolution photometry of ar scorpii: Confirmation of the white dwarf's spin-down. *The Astronomical Journal*, 156(4):150, 10 2018. ISSN 0004-6256. doi: 10.3847/1538-3881/aad5dd. URL https://doi.org/10.3847/1538-3881/aad5dd.

9/10

Appendix

Table 2: Table showing all 30 identified frequencies and their associated amplitude, phase and errors. The accepted, identified frequencies are highlighted in blue.

Index	Frequency (c/d)	Amplitude	Phase	Frequency Error (c/d)
1	6.721	596.5	0.496	0.012
2	3.442	240.8	0.903	0.019
3	9.576	63.81	0.737	0.230
4	12.42	227.6	0.680	0.061
5	14.97	97.90	0.490	0.033
6	20.49	68.64	0.409	0.668
7	24.14	54.64	0.577	0.062
8	26.66	60.30	0.876	0.037
9	30.33	52.58	0.992	0.030
10	38.21	50.57	0.373	11.33
11	45.93	33.68	0.489	604.7
12	56.78	27.68	0.101	0.024
13	60.20	42.13	0.949	0.020
14	71.36	28.92	0.895	3.764
15	78.04	30.15	0.830	0.027
16	725.2	42.93	0.013	1.395
17	731.0	177.0	0.185	0.013
18	737.7	32.93	0.610	0.014
19	744.4	44.09	0.288	0.009
20	1456	41.99	0.649	7.115
21	1462	181.1	0.861	0.007
22	1469	108.6	0.305	0.004
23	1475	129.3	0.892	0.004
24	1482	40.01	0.902	0.010
25	2193	37.91	0.132	0.013
26	2200	31.52	0.379	0.022
27	2206	35.67	0.0187	3.527
28	2937	54.54	0.647	0.016
29	2944	41.00	0.679	6.269
30	2951	37.75	0.503	0.020